

Pixie Dust: Graphics Generated by Levitated and Animated Objects in Computational Acoustic-Potential Field

Yoichi Ochiai*

Takayuki Hoshi†

Jun Rekimoto*‡

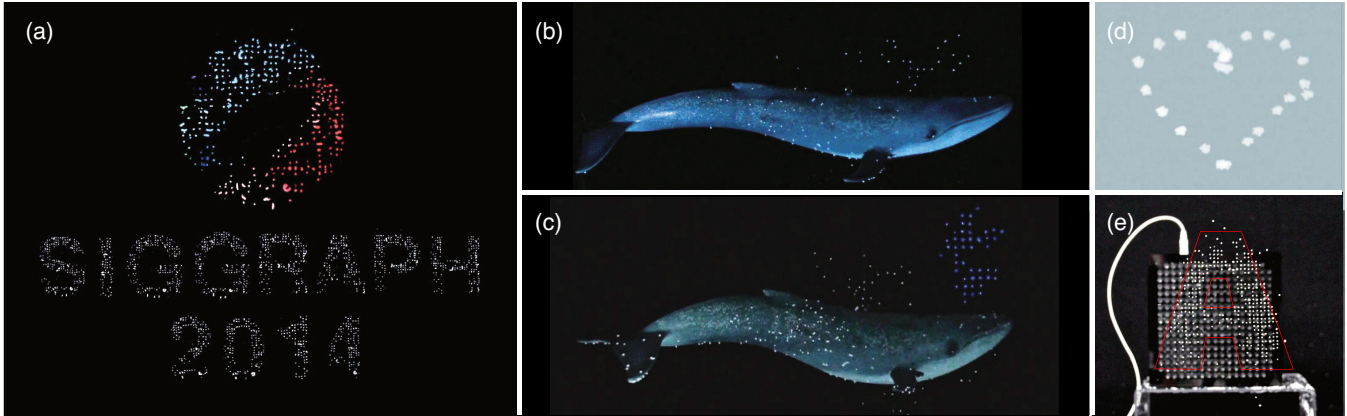


Figure 1: Application images of *Pixie Dust*, levitated and manipulated objects in graphic metaphors. (a) Floating screen with projection. (b-c) Whale (hung by string) with particles and projected spout. (d) Physical vector graphics (showing “heart”). (e) Physical raster graphics.

Abstract

We propose a novel graphics system based on the expansion of 3D acoustic-manipulation technology. In conventional research on acoustic levitation, small objects are trapped in the acoustic beams of standing waves. We expand this method by changing the distribution of the acoustic-potential field (APF). Using this technique, we can generate the graphics using levitated small objects. Our approach makes available many expressions, such as the expression by materials and non-digital appearance. These kinds of expressions are used in many applications, and we aim to combine them with digital controllability. In the current system, multiple particles are levitated together at 4.25-mm intervals. The spatial resolution of the position is 0.5 mm. Particles move at up to 72 cm/s. The allowable density of the material can be up to 7 g/cm³. For this study, we use three options of APF: 2D grid, high-speed movement, and combination with motion capture. These are used to realize floating screen or mid-air raster graphics, mid-air vector graphics, and interaction with levitated objects. This paper reports the details of the acoustic-potential field generator on the design, control, performance evaluation, and exploration of the application space. To discuss the various noncontact manipulation technologies in a unified manner, we introduce a concept called “computational potential field” (CPF).

CR Categories: H.5 [Information interfaces and presentation];

Keywords: Programmable matter, Acoustic manipulation

Links: DL PDF

*The University of Tokyo

†Nagoya Institute of Technology

‡SONY CSL

ACM Reference Format

Ochiai, Y., Hoshi, T., Rekimoto, J. 2014. Pixie Dust: Graphics Generated by Levitated and Animated Objects in Computational Acoustic-Potential Field. ACM Trans. Graph. 33, 4, Article 85 (July 2014), 13 pages.
DOI = 10.1145/2601097.2601118 <http://doi.acm.org/10.1145/2601097.2601118>

Copyright Notice

Permission to make digital or hard copies of all or part of this work for personal or classroom use is granted without fee provided that copies are not made or distributed for profit or commercial advantage and that copies bear this notice and the full citation on the first page. Copyrights for components of this work owned by others than ACM must be honored. Abstracting with credit is permitted. To copy otherwise, or republish, to post on servers or to redistribute to lists, requires prior specific permission and/or a fee. Request permissions from [permissions@acm.org](http://permissions.acm.org).

Copyright © ACM 0730-0301/14/07-ART85 \$15.00.
DOI: <http://doi.acm.org/10.1145/2601097.2601118>

1 Introduction

Interaction with real-world objects is a popular topic in research related to real-world-oriented interactive technologies. In the context of display technologies, analog installations with real objects are still very popular (Figure 2 (b)) in many situations, such as window displays, shops, and museums. Our research in this paper is motivated by the digital control of analog objects in mid-air, i.e., real objects that are suspended and moved in mid-air without physical support, such as posts, rods, and strings (Figure 2 (a)).

Because of growing interest in the materialization of computer graphics, digital fabrication technologies have recently emerged as one of the most important application fields in real-world-oriented computer graphics. These technologies are rapidly expanding from research laboratories to commodity markets for personal use. Fabrication technologies bring computer graphics to the real world. However, two missing and desirable functionalities in digital fabrication are the controllability of spatial position and animation. In the digital world, the spatial position of graphical models is freely controllable by merely setting the coordinates. The ability to do the same in the real world is also desirable for digital fabrication.

We propose in this paper a method to control the spatial position and 3D animation of small objects by utilizing a noncontact manipulation technology. With this method, we can employ real objects as graphical components, such as display pixels (static control) and vector graphics (dynamic control). We believe that a new avenue in the field of computer graphics will be opened if fabricated models can be moved by noncontact manipulation.

Acoustic manipulation has been extended to 3D manipulation [Ochiai et al. 2014]. In this study, we create an acoustic-potential field (APF) by using and extending this technology. Compared to magnetic levitation, air jets, and other noncontact levitation technologies, APF has the following advantages: it can be used with a wide variety of available materials, it provides a satisfactory refresh rate, and it has sufficient spatial resolution. While our technology is limited in terms of the size and density of the objects that are controllable, it contributes to computer graphics by allowing levitated small objects to be used in graphical metaphors, such as the pixels of raster graphics, moving points of vector graphics, and animation.

To discuss various noncontact manipulation technologies in a unified manner, we introduce a concept called “computational potential field” (CPF). We have gathered from literature in the area

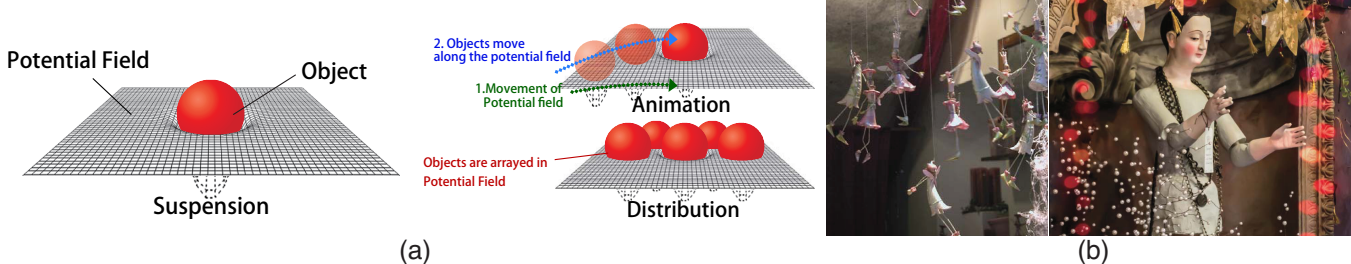


Figure 2: These figures show the concept of computational potential field. (a) Sketch of computational potential field: Objects are trapped in local minima of the potential field. (b) Window installation with objects supported in mid-air. ©DeAnn Peterson ©Ruminatrix

that conventional studies on noncontact levitation/manipulation are based on potential fields determined by various physical quantities, such as sound pressure in acoustic levitation and magnetic fields in magnetic levitation [Brandt 1989]. Levitated objects can be manipulated by spatially and temporally controlling the potential fields. When the field is controlled by a computer, we call it a CPF.

The organization of this contribution is as follows. First, we describe the design of our graphics system. We present the details of the ultrasonic-phased array and discuss its advantages and disadvantages. Second, we report the performance measurements of our system, including the measurements of the spatial resolution, stability, speed of movements, and size and weight of the levitated objects. Finally, we investigate the applications of our system. In addition to the examples of APPF-based graphics applications, we also discuss the implementation of 3D interaction. By integrating a motion-capture system into our graphics system, we facilitate interaction between the levitated objects and the user. Although our investigation is performed using acoustic levitation, our results and discussions can also be useful in designing other CPF-based graphics using other principles of mid-air levitation.

2 Background and related work

In this section, we introduce our motivation for our project and cite related works on noncontact manipulation. Following this, we introduce the concept of CPF to discuss various noncontact manipulation technologies in a unified manner. We then cite related works on acoustic manipulation, passive mid-air screens, and volumetric displays.

2.1 Motivation

Controlling objects in the real world is a popular topic in the computer graphics (CG) and human-computer interaction (HCI) communities. Various ideas to realize this have been proposed – e.g., programmable matter [Goldstein et al. 2005], radical atoms [Ishii et al. 2012], actuation interfaces [Poupyrev et al. 2007], and smart material interfaces [Nijholt et al. 2012]. These proposals focus on controlling real objects through a computer and generating physically programmable material. These concepts will play very important roles in future interactive CGs because they expand the range of graphics from “painted bits” to the real world [Ishii and Ullmer 1997].

Two methods are currently available to control objects in the real world. In one, objects actuate themselves, whereas they are actuated by their surroundings in the other. The latter method is divided into two types of actuation: contact and noncontact. We address the noncontact approach.

2.2 Manipulation methods in interactive techniques

Several related studies have aimed at noncontact manipulation in the context of interactive techniques. For example, ZeroN [Lee et al. 2011] was proposed to manipulate a 3D object by controlling the magnetic field and using it as a floating screen and an input user interface (UI). The levitated object is limited to a single magnetic sphere in this proposal. Noncontact manipulation can be also achieved by using air-jets [Iwaki et al. 2011], i.e., an airflow field. While the research is limited to 2D manipulation, it can be extended to 3D. Air-cannons [Sodhi et al. 2013] have a possibility to be used in the similar manner. Sound is also utilized to manipulate objects in air. Both of standing waves (acoustic levitation/manipulation) and traveling waves (e.g., Ultra-Tangibles [Marshall et al. 2012]) are available. A comparison of these manipulation methods is shown in Table 1.

2.3 Computational potential field

We propose a new implementation concept – computational potential field (CPF). We use the term “potential field” in a narrow sense: a scalar field that gives a force vector field working on a given object. Then CPF is defined as a potential field determined by some physical quantities controlled by a computer that can suspend and move objects in the real world. To the best of our knowledge, all conventional research on noncontact manipulation can be classified as CPF. All studies in the area employ CPFs as “invisible strings” to manipulate real objects. In these implementations, the objects have no actuators and only float in air according to the spatiotemporal changes of the CPF.

2.4 Acoustic manipulation

Several studies have been conducted on manipulation using ultrasonic waves. For example, Ultra-Tangibles [Marshall et al. 2012] utilizes the acoustic radiation pressure of traveling waves from the surrounding ultrasonic-phased arrays. Marshall et al. demonstrated 2D manipulation of lightweight spherical objects. Another method

Table 1: Comparative table of manipulation methods.

Physical quantity	Material parameters	Mechanism	Spatial resolution
Sound	Density & volume	Ultrasonic transducers	Wave length
Airflow [Iwaki et al. 2011]	Density & surface area	Air jets	Spread of air jets
Magnetism [Lee et al. 2011]	Weight & magnetism	Electromagnet & XY stage	Size of magnet

– acoustic levitation/manipulation – utilizes ultrasonic standing waves. A bolted Langevin transducer (BLT) is used together with a reflector to trap objects in water and levitate them in air [Xie et al. 2006; Kozuka et al. 2007]. Opposite BLTs were used to manipulate objects in a 1D direction along the acoustic beam [Kozuka et al. 2007; Weber et al. 2012]. Acoustophoretic transport [Foresti et al. 2013] and lapillus bug [Kono et al. 2013] move the object along a 2D plane with a transducer array and a reflector plate. Extended acoustic manipulation [Ochiai et al. 2014] moves objects in a 3D space with opposite transducer arrays, but no application of this method has been suggested.

In this study, we aim to describe the extension and application of acoustic levitation and manipulation to the fields of CG and HCI. One difference between our proposal and conventional methods in the area is that we control the shape of the beams. Furthermore, multiple objects can be levitated and manipulated together in a 3D space using our method. Our system can also make a dot matrix display in mid-air. These differences from related research are depicted in Figure 3. The limitations of our system are described in Section 3.

2.5 Passive mid-air screens

Studies that have been conducted on dealing with mid-air screens are listed. Many image-projection technologies have been investigated. The systems proposed by [Rakkolainen et al. 2005; Lee et al. 2009] use fog as a screen and the one by [Perlin and HAN 2006] uses dust-like particles as a screen. These technologies display images in air by utilizing the diffusion property of fog and dust. [Barnum et al. 2010] has developed a screen that uses falling water drops in air. Utilizing their lens-like property, images are able to be projected onto them. Multilayer water-drop screens are created in air and images corresponding to the spatial position of the water drops are projected by synchronizing the projector with the water bulbs. In the aspect of passive floating display using water, there is [Heiner et al. 1999] which is the display aimed to realize ambient display. Our study differs from these studies in the spatial control and selectivity of the available material, and can also expand these passive screen approaches.

2.6 Volumetric displays and screens

Studies directed toward controlling the spatial position of an active screen and display are also being actively pursued. There are two kinds of the studies; one aims to achieve multi-perspective 3D image and the other aims to realize deformation of planer screens for haptic and/or other purposes. Multi-perspective 3D dis-

play is a popular topic in computational display areas. We would like to cite several researches from the viewpoint of volumetric display. [Jones et al. 2007] constructs 3D images with a rotated mirror and projection. [Cossairt et al. 2007] achieves 3D images by rotating a vertical diffuser plate and projection. [Wetzstein et al. 2011] is glasses-free light field display using volumetric attenuators. On the other hand, there are researches that focus on the dynamic deformable screen and display. For example, the deformable actuated screen “Project FEELEX” [Iwata et al. 2001] constructs 3D forms on the screen surface using an actuator array set under the screen. LUMEN, proposed by [Poupyrev et al. 2004], is comprised of actuated dot-matrix light-emitting diode (LED) – physical pixels showing RGB and H (height). [Follmer et al. 2013] has proposed an interactive deformable screen, called “inForm,” that handles and/or interacts with other objects. A noncontactly-actuated deformable screen [Ochiai et al. 2013] employs an ultrasonic-phased array to deform a colloidal screen. Our approach differs from these screens and displays in that it allows for 3D manipulation and levitation. Moreover, we can use various materials as volumetric pixels. While there is a 3D solution [Kimura et al. 2011] that uses a plasma 3D volumetric display, our approach is different from it because of the fact that volumetric pixels are touchable in our approach.

3 Acoustic-potential field generator

In this section, we describe the theory of our acoustic-potential field generator. It consists of ultrasonic-phased arrays surrounding the workspace. First, we explain how to make a focal point/line with an ultrasonic-phased array. Then, we describe the distribution of the ultrasonic-acoustic-potential field.

3.1 Ultrasonic-phased array

The acoustic-potential field generator consists of multiple modules of ultrasonic-phased array. Each module has hundreds of ultrasonic transducers and controls each separately with adequate time (or phase) delays. In [Ochiai et al. 2014], a similar setup was used to levitate and manipulate small particles and each module generated a focal point. In this study, we use this setup to generate not only a single focal point, but also other distributions of ultrasound, e.g., multiple focal points [Carter et al. 2013] and a focal line. In the following sections, we explain how to generate the focal point and focal line. Their spatial distributions are also shown.

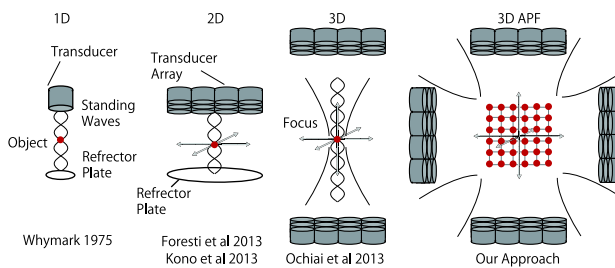


Figure 3: The differences in acoustic manipulation approaches. (a) Simple standing wave levitation. (b) 2D manipulation of small particles with transducer array. (c) 3D manipulation using opposite phased arrays. (d) 3D manipulation and deformation of Acoustic-Potential Field: our approach.

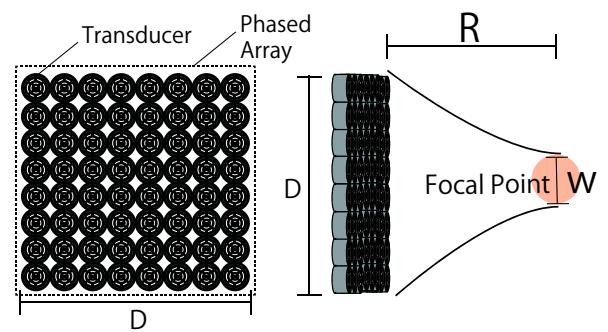


Figure 4: Phased array with side length D and focal length R .

3.1.1 How to generate focal point

A focal point of ultrasound is generated as follows. The time delay Δt_{ij} for the (i, j) -th transducer is given by:

$$\Delta t_{ij} = (l_{00} - l_{ij})/c \quad (1)$$

where l_{00} and l_{ij} are the distances from the focal point to the $(0, 0)$ -th (reference) and the (i, j) -th transducers, respectively. c is the speed of sound in air. The focal point can be moved by recalculating and setting the time delays for its next coordinates.

It has been theoretically and experimentally shown that the spatial distribution of ultrasound generated from a rectangular transducer array is nearly sinc-function-shaped [Hoshi et al. 2010]. The width of the main lobe w parallel to the side of the rectangular array is written as

$$w = \frac{2\lambda R}{D} \quad (2)$$

where λ is the wavelength, R is the focal length and D is the length of the side of the rectangular array (Figure 4). This equation implies that there is a trade-off between spatial resolution and the array size.

3.1.2 How to generate focal line

A focal line of an ultrasound is generated in a similar manner with variation in the target coordinates. In this case, the time delay Δt_{ij} for the (i, j) -th transducer is given by:

$$\Delta t_{ij} = (l_{0j} - l_{ij})/c \quad (3)$$

where l_{0j} and l_{ij} are the distances from the j -th focal point to the $(0, j)$ -th and the (i, j) -th transducers, respectively, i.e., each column targets its own focal point (Figure 6). The thickness of the focal line is w , as defined in Eq. (2) above. The peak value of the amplitude of the focal line is lower than that of the focal point because the acoustic energy is distributed over a broader area.

3.2 Acoustic-potential field

The principle of acoustic levitation was mathematically explained by [Gor'kov 1962] and [Nybørg 1967]. When a small sphere is in an acoustic field, the potential energy U of an ultrasonic standing wave is expressed as

$$U = -B\langle K_a \rangle + (1 - \gamma)\langle P_a \rangle \quad (4)$$

K_a and P_a here are the kinetic and potential energy densities of ultrasound, respectively. $\langle \rangle$ is the time average. B is given by $3(\rho - \rho_0)/(2\rho + \rho_0)$, where ρ and ρ_0 are the densities of a small sphere and the medium, respectively. γ is given by β/β_0 where β and

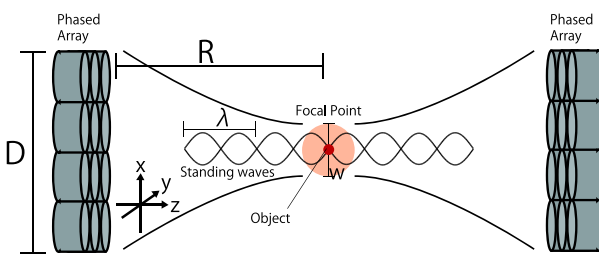


Figure 5: Opposite phased arrays, focal points, and standing wave.

β_0 are the compression ratios of the small sphere and the medium, respectively. The force F acting on a sphere of volume V is given by $F = -V\nabla U$. In the following, we show the potential fields for a focal point and a focal line.

3.2.1 Focal point

A narrow beam of standing wave is generated in the vicinity of a focal point when two phased arrays are set opposite each other and generate the common focal point (Figure 5). The length of the standing wave depends on the focal depth.

We assume an ultrasonic standing wave along the z -axis. Its sound pressure p is written as

$$p = \sqrt{2}Ag(x, y) \cos\left(\frac{2\pi z}{\lambda}\right)e^{-j\omega t} \quad (5)$$

where A is the root mean square (RMS) amplitude, $g(x, y)$ is the normalized cross-sectional distribution of the ultrasonic beam, and ω is the angular velocity. By definition, $K_a \equiv \frac{\rho u^2}{2}$ and $P_a \equiv \frac{p^2}{2\rho c^2}$ where u is the particle velocity. In the beam of standing wave, $u = \frac{1}{\rho c} \frac{\partial p}{\partial z}$. Then, U is written as

$$U = g(x, y)^2 \frac{A^2}{\rho_0 c^2} \left\{ -B + (B + 1 - \gamma) \cos^2\left(\frac{2\pi z}{\lambda}\right) \right\} \quad (6)$$

As we mentioned above, it has been theoretically determined that the distribution of the focal point $g(x, y)$ generated by a rectangular transducer array can be approximated by a sinc function [Hoshi et al. 2010].

$$g(x, y) \simeq \text{sinc}\left(\frac{2\pi x}{w}, \frac{2\pi y}{w}\right) \quad (7)$$

where the two-dimensional sinc function $\text{sinc}(x, y)$ is defined as $\sin(x)/xy$.

Figure 7 shows the potential energy distribution based on Eqs. (6) and (7) for $y = 0$. It is assumed here that the sphere is made of polystyrene and the medium is air. Hence, $\rho = 1 \times 10^3 \text{ kg/m}^3$, $\rho_0 = 1.2 \text{ kg/m}^3$, $\beta = 2.5 \times 10^{-10} \text{ Pa}^{-1}$, and $\beta_0 = 7.1 \times 10^{-6} \text{ Pa}^{-1}$. The figure shows that the small spheres gravitate toward the acoustic axis of the ultrasound beam at its nodes. Figure 7 (b) and (c) show the particles levitated and animated in this potential field.

3.2.2 Focal line

A sheet beam of standing wave is generated in the vicinity of a focal point when four phased arrays surround the workspace and generate

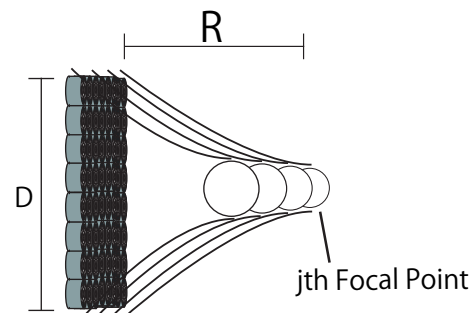


Figure 6: Generation of focal line.

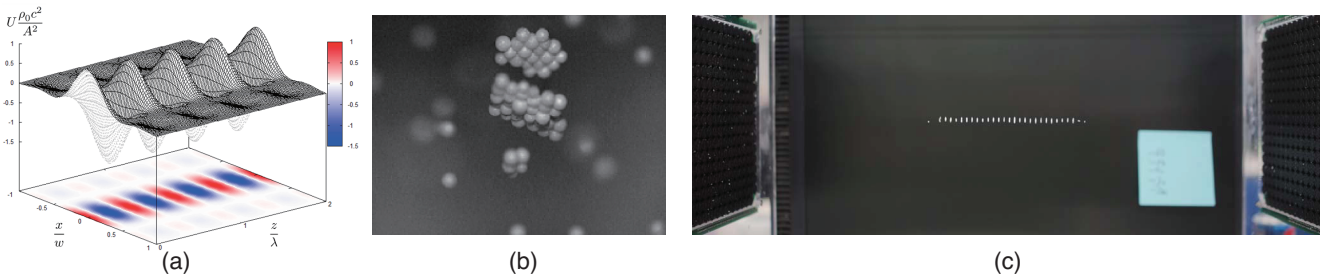


Figure 7: (a) Potential field in the vicinity of the focal point of the ultrasonic beam. (b) Small particles captured by 4000-fps high speed camera (200×). (c) Small particles trapped in potential field.

focal lines at the same position. This acoustic field is described as two beams of standing waves that overlap perpendicular to each other.

We assume an ultrasonic standing wave parallel to the x and z axes. Its sound pressure p is written as:

$$p = \sqrt{2}A\sin(\frac{2\pi y}{w})\{\cos(\frac{2\pi x}{w}) + \cos(\frac{2\pi z}{w})\}e^{-j\omega t} \quad (8)$$

Then, U is written as:

$$\begin{aligned} U &= \sin^2(\frac{2\pi y}{w})\frac{A^2}{\rho_0 c^2}\{-B[\sin^2(\frac{2\pi x}{\lambda}) + \sin^2(\frac{2\pi z}{\lambda})] \\ &\quad + (1-\gamma)[\cos(\frac{2\pi x}{\lambda}) + \cos(\frac{2\pi z}{\lambda})]^2\} \end{aligned} \quad (9)$$

Figure 8 shows the potential energy distribution based on Eq. (9) for $y = 0$ under the same conditions as in Section 3.2.1. The potential field has equally spaced local minima. This is used to create a dot matrix of small particles.

3.3 Setup Variations

The intensity of the suspending force depends on the direction of the acoustic beam relative to gravity. Here, we derive and compare two extreme situations of a narrow beam: a vertical and a horizontal setup. The axial force F_z counters gravity in the vertical setup (Figure 9 (a)) and the radial force F_x in the horizontal setup (Figure 9 (b)). For simplicity, we assume $B \approx 3/2$ and $\gamma \approx 0$, because $\rho \gg \rho_0$ and $\beta \ll \beta_0$ for our case.

First, the radial force F_x parallel to the x-axis through the center of

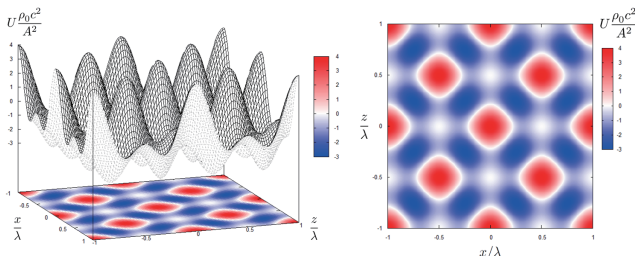


Figure 8: Potential field in the vicinity of the intersection of the ultrasonic sheet beams.

a node is obtained as:

$$\begin{aligned} F_x &\equiv \dots - V \frac{\partial U}{\partial x} |_{(y,z)=(0,\frac{\lambda}{4})} \\ &\approx \frac{A^2 V}{\rho_0 c^2} \frac{6\pi}{w} \left[\frac{\sin(\frac{2\pi x}{w}) \cos(\frac{2\pi x}{w})}{(\frac{2\pi x}{w})^2} - \frac{\sin^2(\frac{2\pi x}{w})}{(\frac{2\pi x}{w})^3} \right] \end{aligned} \quad (10)$$

The maximum value of F_x/Vg is 5×10^3 kg/m³ at $x \approx -0.2\lambda$, where $g = 9.8$ m/s² is the gravitational acceleration and $A = 5170$ Pa. This means that a material can be levitated by F_x if its weight density is smaller than this value. For example, the weight density of polystyrene is approximately 1×10^3 kg/m³.

Second, the axial force F_z along the z-axis is obtained as:

$$\begin{aligned} F_z &\equiv \dots - V \frac{\partial U}{\partial z} |_{(x,y)=(0,0)} \\ &\approx \frac{A^2 V}{\rho_0 c^2} \frac{10\pi}{\lambda} \sin(\frac{2\pi z}{\lambda}) \cos(\frac{2\pi z}{\lambda}). \end{aligned} \quad (11)$$

The maximum value of F_z/Vg is 3.63×10^4 kg/m³ at, for example, $z = \lambda/8$. The maximum value of F_z is 7.3 times larger than that of F_x , as derived above. This estimation agrees with the report that lateral restoring forces are approximately 10 times larger than the main sound beam [Whymark 1975], and explains why F_z , rather than F_x , was primarily used in conventional studies.

In this study, we can also utilize F_x to levitate objects because we have sufficient high-amplitude ultrasound owing to phased arrays. Note that not only the weight density but also the size and shape of the objects are important factors to determine if they can be trapped in the nodes.

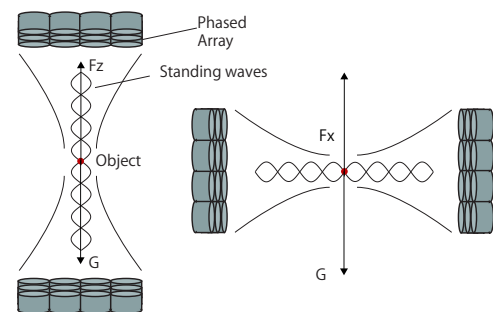


Figure 9: The force against the gravity. (a) Vertical setup. (b) Horizontal setup.

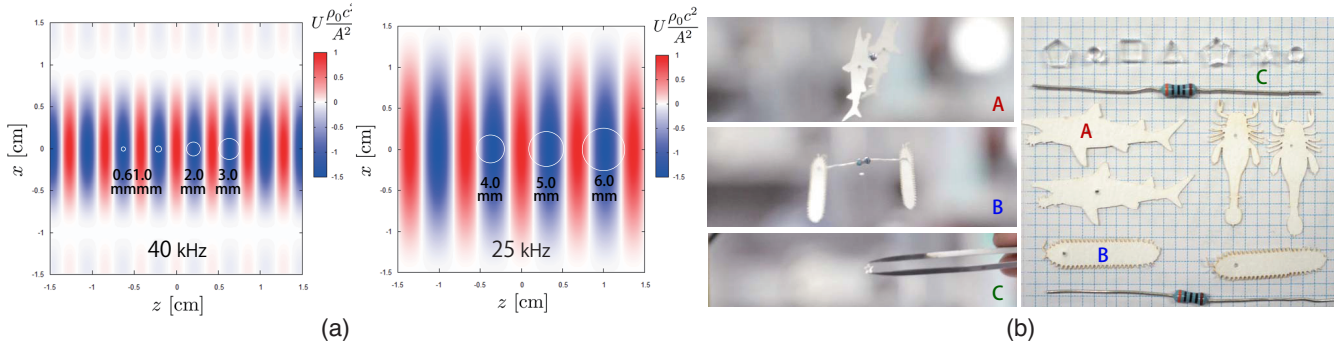


Figure 10: (a) Node size vs. frequency of ultrasound. White circles show particles in various diameter. (b) Floating paper models fabricated by laser cutter.

3.4 Frequency and size of floated objects

The node size depends on the frequency of the ultrasound and determines the allowable size of the floated objects (Figure 10 (a)). The interval between the nodes is $\lambda/2$ and the size of the node is $\lambda/2$ by the width of the ultrasonic beam w . For example, $\lambda/2 = 4.25$ mm when we select 40 kHz. The frequency should be determined according to the intended application. Note that this is a rough standard, and that objects larger than the node size can be levitated if the protrusion is small/light enough to be supported by the suspending force (Figure 10 (b)).

3.5 Shape of potential field

We have discussed two types of potential fields above: a focal point and focal line. Note that phased arrays control transducers individually and can generate other distributions of potential fields, such as multiple beams. The arrangement of the phased arrays can be used to design the shape of the potential field. Figure 11 shows examples of the computational acoustic-potential field, where the particles indicate the local minima (nodes) of the potential fields.

4 Implementation and evaluation

In this section, we describe the implementation of the acoustic-potential field generator that consists of phased arrays. We then show the results of the experiments and the measurements of the acoustic-potential field generator.

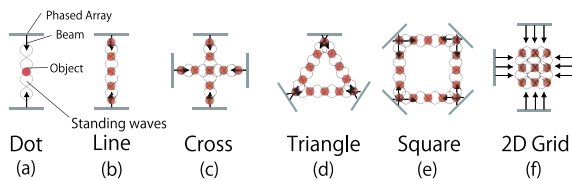


Figure 11: Multiple beams and different shapes of potential field. (a) Dot by a pair of phased arrays. (b) Line by a pair of phased arrays. (c) Cross by two pairs of phased arrays. (d) Triangle by three phased arrays. (e) Square (with multiple beams) and (f) dot-matrix (with wide beams) by two pairs of phased arrays.

Table 2: 40-kHz and 25-kHz ultrasonic phased arrays.

	40 kHz	25 kHz
Number of transducers	285 pcs	100 pcs
Sound pressure	2585 Pa RMS (measured)	900 Pa RMS (estimated)
Size of nodes	4.25 mm	6.8 mm

4.1 Phased array modules

We developed our manipulation system with four modules of phased array [Hoshi 2012], as shown in Figure 12. The surrounded area is 520×520 mm². We placed the phased arrays facing each other.

We have two options of phased arrays with different frequencies (40 and 25 kHz; Table 2). The position of the focal point is digitally controlled with a resolution of 1/16 of the wavelength (approximately 0.5mm for the 40-kHz ultrasound) and can be refreshed at 1kHz. The 40-kHz phased array consists of 285 transducers (10-mm diameter, T4010A1, Nippon Ceramic Co., Ltd.) arranged in a 170×170 mm² area. The sound pressure at the peak of the focal point is 2585 Pa RMS (measured) when the focal length $R = 200$ mm. The 25-kHz phased array consists of 100 transducers (16-mm diameter, T2516A1, Nippon Ceramic Co., Ltd.). The sound pressure at the peak of the focal point is 900 Pa RMS (estimated) when the focal length $R = 200$ mm. Using 25-kHz phased arrays, the suspending force is much smaller while the size of the focal point is larger. In this study, we primarily use 40-kHz phased arrays to obtain a larger suspending force.

The size and weight of a single phased array are $19 \times 19 \times 5$ cm³ and

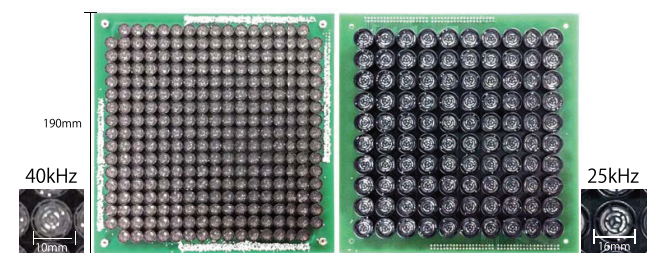


Figure 12: Phased arrays. (Left) 40 kHz and 285 pcs. (Right) 25 kHz and 100 pcs.

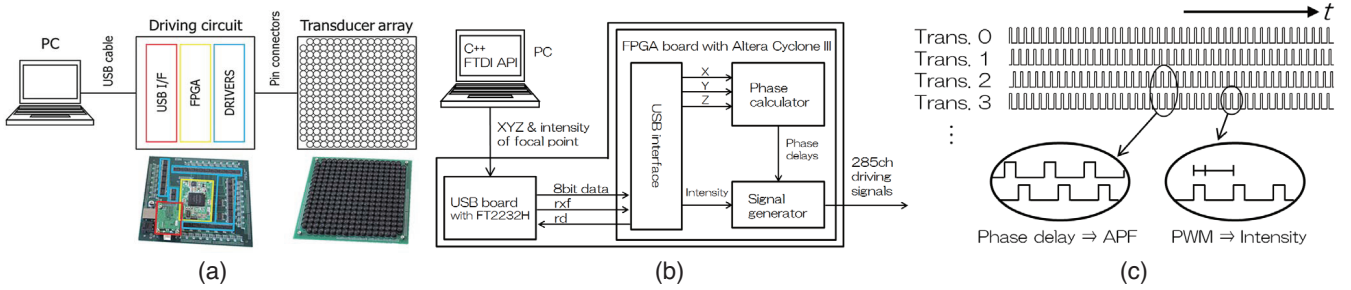


Figure 13: (a) System overview. (b) Diagram of data-flow. (c) Control of focusing (or distribution of acoustic potential field) and output intensity.

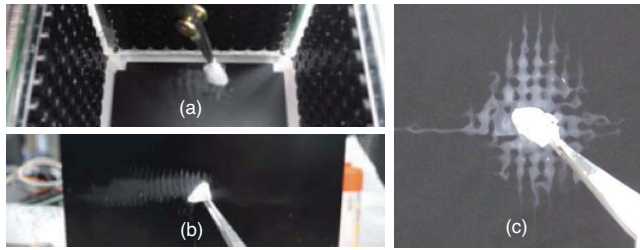


Figure 14: Visualization of ultrasonic beams by dry ice. (a) 25 kHz, (b) 40 kHz, and (c) 2D grid of 40 kHz.

0.6 kg, respectively. It consists of two circuit boards. One is an array board of ultrasonic transducers and the other is a driving board, including an FPGA and push-pull amplifier ICs. These boards are connected to each other with pin connectors.

The phased array is controlled by a single PC via USB. The control application is developed in C++ on Windows (Figure 13). The PC sends the data, including the coordinates of the focal point and output intensity, to the driving board. The driving board receives the data, calculates adequate time delays for each transducer based on Eqs. (1) or (3), and generates the driving signals. The driving signals are sent to the transducers via the amplifiers. Modifying the time-delay calculation algorithm changes the distribution of the acoustic-potential field. The output intensity is varied using pulse-width modulation (PWM) control of the driving signal.

4.2 Control method for manipulation and animation

We detail here our control method using the APF to manipulate levitated objects. The narrow beams, or sheet beams, of standing wave are generated in the vicinity of a single target point in our current setup. The APF changes according to the movement of this target point and then moves the levitated objects. Note that all the levitated objects are moved together in the same direction in this control method.

The movement of the target point should be as continuous as possible to keep the objects levitated. If the distance between the old and new target points is large, the levitated objects cannot follow the change in the APF. Note that although the APF generator has a 0.5-mm spatial resolution and a 1-kHz refresh rate, the inertia of the levitated objects limits the speed of their movement. This capability is investigated in Section 4.3.2.

4.3 Experimental measurements

4.3.1 Visualization of beams

Here, we visualize the acoustic field by placing dry ice near it. The air inside the ultrasonic beam is cooled and the moisture is frozen and visible. The micro-particles of ice gather at the local minima of the acoustic-potential field. Figure 14 shows the ultrasonic beams of standing waves of 25 kHz and 40 kHz. In both cases, the interval between the nodes is $\lambda/2$.

4.3.2 Experiment on speed of manipulation

We examined the speed of manipulation attained by the current setup by measuring the duration of the cyclical movement at different frequencies. The test was conducted using expanded-polystyrene spheres of diameters 0.6 mm and 2 mm. In each trial, a single particle was set at the third node from the intersection of the ultrasound beams along one of the acoustic axes (x-axis). All the directions of movement (i.e., x along an acoustic axis in which the particle is trapped, z along the other axis, and y perpendicular to both the axes) were tested. The focal length was set at 260 mm (Figure 15 (a)). The sound pressure was set to 70The amplitude of the cyclic movement was 15 mm. Figure 15 (b)–(d) shows the results. The points on the graph indicate the average floating time for the different frequencies, and the bars indicate the maximum and minimum values. It can be observed that manipulation along the y-axis was more stable than along the other axes. We speculate that manipulations along the x and z axes tend to induce discontinuity in the ultrasound to change the focal length. Moreover, the graph shows that particles with diameter 0.6 mm are more stable than those with diameter 2 mm at higher frequencies. This suggests that larger particles tend to fall from the nodes of a standing wave.

4.3.3 Experiment on workspace

We examined the size of the workspace in which the particles are suspended. The experiment begins with the center position. Each beam has 14–19 nodes that are occupied by the particles. The experimental setup is shown in Figure 16. The figure shows how a particle falls when the focal point moves to a more distant position. The x-axis shows the distance from the center and the y-axis shows the number of nodes that include particles with a 0.6-mm diameter.

The workspace was studied next. In the case of movement along one of the acoustic axes, the manipulated particles could approach the ultrasound array to within 60 mm, but dropped when the distance became smaller. In the case of movement perpendicular to the acoustic axes, the particles at the more distant nodes dropped earlier when they moved away from the center of the system. A

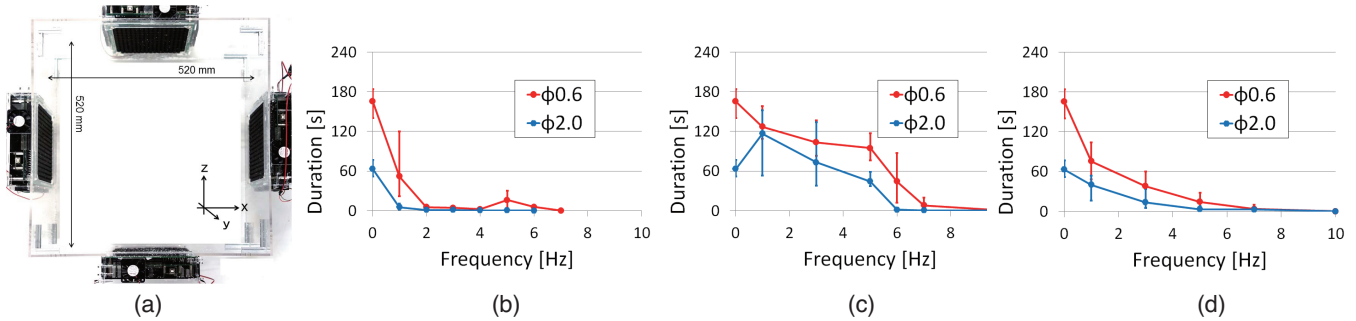


Figure 15: (a) Experimental setup and results on speed of manipulation. (b) Parallel to x-axis. (c) Parallel to y-axis. (d) Parallel to z-axis.

particle at the intersection of the ultrasound beams dropped when it came to within 330 mm of the center.

4.3.4 Experiment on weight capability

We examined the capability of levitation with various materials. We employed nuts made of several materials and sizes. We levitated them in the center of the node in the vertical and horizontal setup. The results are shown in Figure 17. The weight capability is calculated from the size and density: vertical F_z can hold up to 1.09 g and horizontal F_x can hold up to 0.66 g. The relationship between the amplitude of the ultrasound and mass is also plotted in Figure 17.

While we concluded that our system can suspend up to 1.09 g and 0.66 g, there are other factors to be considered in addition to the weight of objects – namely, the shape of objects, the intensity of the ultrasound, and the geometry of the APF.

5 Applications and results

In this section, we discuss the application of the proposed method. First, we describe the characteristics of the method. We then outline the possible applications: graphics and interactions based on the acoustic potential field (APF) of wide/narrow ultrasonic beams.

5.1 Characteristics

The levitation and manipulation method used in our study has several characteristics that can prove useful in graphics applications. These include

1. Simultaneous levitation and manipulation of multiple objects by modification of APF
2. Rapid manipulation of levitated objects resulting in the production of persistence of vision
3. Only dimension and density limitations on levitating objects

In this paper, we introduced two options, wide and narrow beams. The wide beam is used for projection screens and raster graphics, whereas the narrow beam is used for the levitation of various objects and vector graphics. Furthermore, other applications – animation of real objects, interaction with humans, particle effects, and pseudo high-screen resolution – can be implemented. Figure 20 shows a map of the applications placed according to their speed of motion.

5.2 Graphic application with grid-like APF

In this application, a 2D grid APF generated by wide beams, depicted in Figure 11 (f), is used as a projection screen floating in mid-air. Moreover, raster graphics images are generated when adequate particles are blown off.

5.2.1 Projection screen

Figure 18 shows a floating screen, with the 2D grid APF suspending small particles in all the nodes. The movement of the screen has a high refresh rate and high spatial resolution. In our current prototype, the maximum control rate is 1 kHz, the distance between the particles is 4.25 mm, and 85×85 particles are held at the maximum. This kind of mid-air floating screen is applicable for use in areas such as entertainment, show windows, and interior displays.

Conventional proposals include fog screens [Rakkolainen et al. 2005], water drop screens [Barnum et al. 2010], and fog-filled bubble screens [Nakamura et al. 2006]. However, these are mid-air, passive projector screens. Our proposed system differs from these in that the spatial position of our screen is controllable and the screen objects can be selected according to usage (Figure 19 (b)). Our system can also expand conventional systems by, for instance, suspending water drops, holding fog particles, and controlling soap bubbles in the air.

Furthermore, the screen can be moved three-dimensionally as well as manipulation and animation applications. There are two types of effects: The movement vertical to the screen results in volumetric expression and that parallel to the screen achieves pseudo high resolution.

5.2.2 Levitated raster graphics

Figure 19 (c) shows a raster graphics display. First, the APF suspends small particles in all nodes to the same extent as in Section 5.2.1. The system then adequately blows off some of the particles and generates a raster image. This process is performed by an additional phased array, or air jet. The accuracy of dropping particles is approximately 2 cm by phased array and a single pixel by air jet at close range. The control rate of movement and spatial resolution of pixels are the same as in Section 5.2.1.

There are several studies that focus on mid-air displays. For example, [Kimura et al. 2011] is a 3D volumetric display based on laser-excited plasma that generates an image consisting of luminous points. Our system differs from this to the extent of non-luminous and physical-material pixels. A projector is not necessarily needed and the natural appearance of a real object is used as an expression. The availability of a non-luminous mid-air display in addition to a

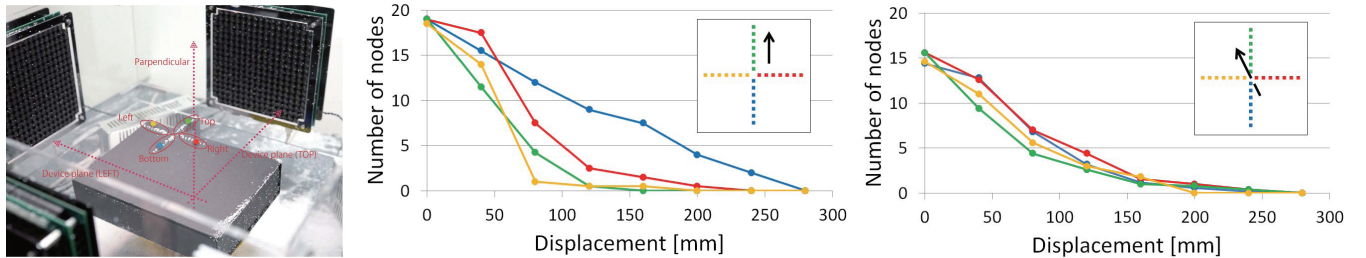


Figure 16: Experimental results on size of workspace. Left graph shows movement along acoustic axis and right graph shows movement perpendicular to device plane.

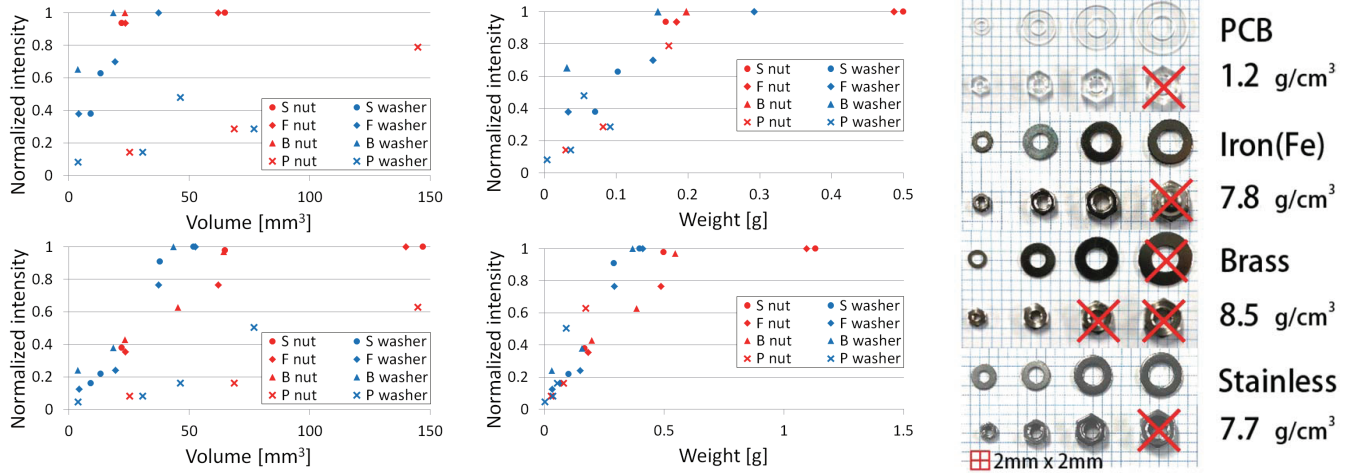


Figure 17: Experimental results (nuts and ring washers). (Left) The horizontal axis shows the volumes and weights of objects. The vertical axis shows the normalized intensity of ultrasound. The upper and lower graphs show horizontal and vertical setup, respectively. The labels S, F, B, and P are Stainless, Iron (Fe), Brass, and PCB, respectively. (Right) Levitated objects (the objects marked with “x” were not levitated).

conventional luminous mid-air display is useful for design contents and installation.

5.3 High-speed animated APF

We focus here on a cross APF generated by the narrow beams shown in Figure 11 (a)–(c). By changing the spatial position of the nodes of the APF (either points or lines), the levitated objects are moved. The movement is fast enough to turn the trajectories of the objects into vector graphics based on persistence of vision. Figure 21 (a) and (b) show the results.

5.3.1 Physical vector graphics

By moving particles quickly, a vector graphics display is achieved based on persistence of vision. We used two types of particles as moving particles: 1-mm luminous painted balls and 1-mm polystyrene particles. In the case of the luminous painted balls, we first irradiated light onto the balls and then manipulated them quickly mid-air. The trajectories are designed as a series of coordinates of control points, which are set up to 1,000 points-per-second. As the results of the above experiments showed, the maximum speed of movement was 72 cm/s. This speed is enough to produce persistence of vision. Figure 21 (a) and (b) show the results.

Research has been conducted on long-exposure photographs of LED lights [TOCHKA] and LED-decorated quad-copters [Landis 2013]. However, our study differs from them in that vector graphics in mid-air are rendered in real time and non-luminous images are

obtained with polystyrene balls.

5.3.2 Physical particle effects

The movement of the APF produces not only vector graphics, but also particle effects in the real world (Figure 21 (c)). The temporal change in the APF affects the trajectories of falling particles, and the trajectory changes of multiple particles visualize the APF change. The speed of the movement is the same as in Section 5.3.1.

5.4 Animation and interaction

Both 2D grid and cross APFs offer animation of levitated objects and/or interaction between users and levitated objects. Our study animates “passive” and “real-world” objects based on a noncontact manipulation method (Figure 24). We combined our levitation and manipulation setup with an IR-based motion capture system. When we levitated and manipulated small retro-reflective balls, all the balls were tracked by the motion capture system. Results are shown in Figure 22 (Left), in which we used a single 1-mm retro-reflective ball and levitated it.

Another motion capture setup was developed with Kinect. In this setup, users are detected without any attachments on their bodies and the levitated objects are controlled according to the motion of the users’ hands. An illustration of its use is given in Figure 22 (Right).



Figure 18: Mid-air screen with projection (showing SIGGRAPH logo, S, I, G, G, R, A, P, and H).

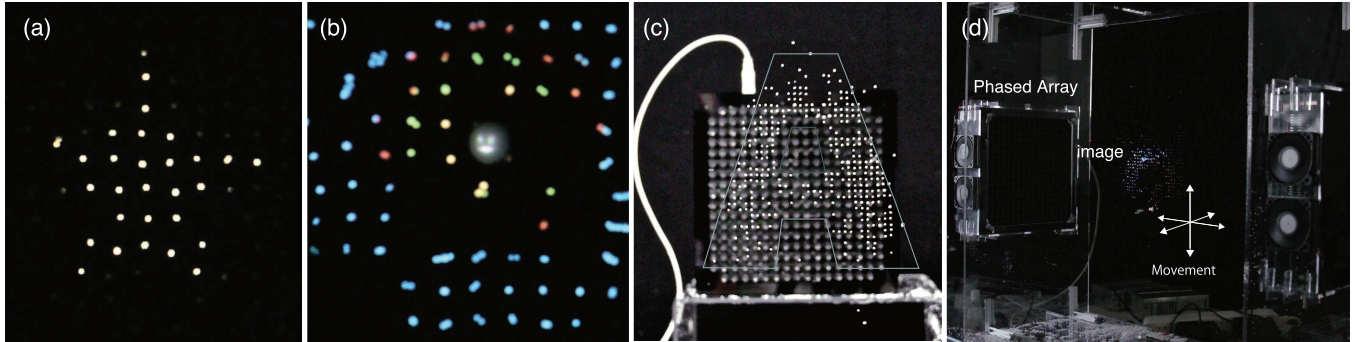


Figure 19: (a) Mid-air screen with another projection (“Star”). (b) Mixture of objects of different sizes (a detailed image is projected on larger particle). (c) Physical raster graphics (showing “A”). (d) Setup of mid-air screen and physical raster graphics.

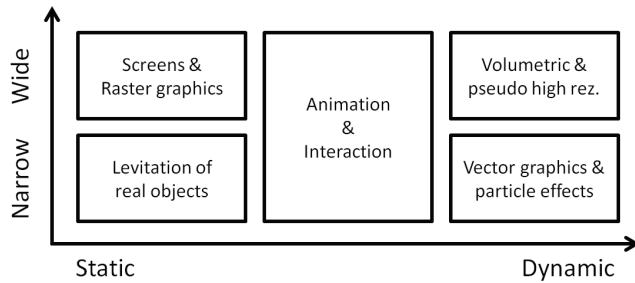


Figure 20: Application domain.

6 Discussions

6.1 Limitations

6.1.1 Material limitation

There are two factors to consider when choosing objects to manipulate: dimension and density. The allowable dimension is determined by the geometry of the APF and the allowable density of the material is related to the intensity of ultrasound. In Section 3, the maximum density of a levitated object is theoretically derived as $5 \times 10^3 \text{ kg/m}^3$. Examples of materials that satisfy this condition include light metals and liquids. As described in Section 3, the size limitation (the size of nodes) is determined by the frequency of ultrasound: 4.25 mm for 40 kHz and 6.8 mm for 25 kHz. A lower frequency leads to larger size. Internal force is also an important factor in selecting the material. For example, the electrostatic force determines the maximum number of particles that can be trapped in a single node. The surface tension of the fluid determines the size of the droplets that can be levitated. Further, the shape of the levitated object is limited by the shape of the node.

6.1.2 Sustainability of suspension

Three factors determine the sustainability of the suspension: the heat condition of ultrasonic devices, oscillation of objects inside the nodes, and acceleration in vector graphics. In this section, descriptions of the factors and the ways to cope with them are provided.

The difference in the heat condition of the ultrasonic devices causes a single standing wave to affect the sustainability of the suspension. The temperatures of devices are equivalent prior to them being turned on. When they are turned on, their temperatures gradually increase because of the heat generated by amplifier ICs whose characteristics are not fully equivalent. When there is a difference in temperature, the operating frequencies of the controlling circuits differ. The frequency difference causes transportation of the nodes and the levitated objects fall off when they reach the edge of the localized standing wave. The cooling and maintenance of the temperature balance of the devices is one treatment. Another is to adjust phase delays based on feed-forward or visual feedback control.

Oscillation of levitated objects is another factor to be considered. When some kind of fluctuation occurs on the object, it suffers the restoring force from the potential field. If the intensity of the ultrasound is too high, the oscillation grows and finally exceeds the node of the potential field. The oscillation is restrained by decreasing the intensity of the ultrasound keeping it suspended.

When moving levitated objects, the acceleration acts to throw them off the nodes. This determines the possible shapes and sizes of the physical vector graphics. Increasing the intensity of ultrasound at sharp curves would elongate the drawing time and expand the variation of physical vector graphics.

In practice, it is acceptable in many cases to refill objects into the APF if necessary.

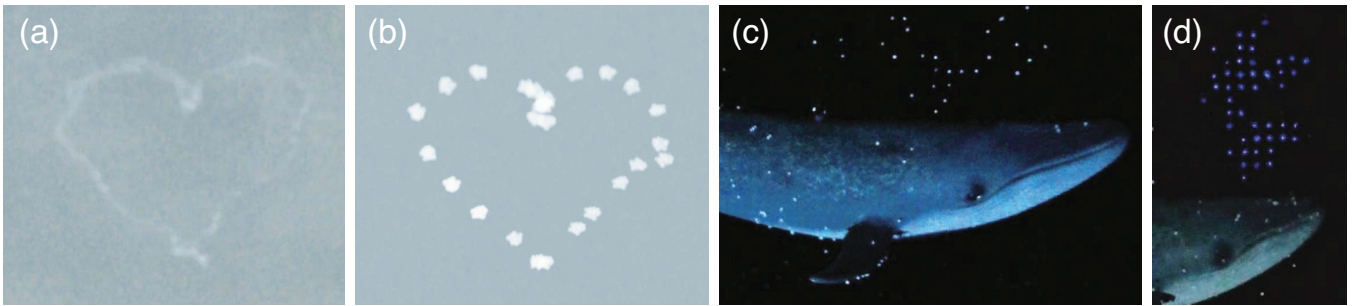


Figure 21: (a) Physical vector graphics (“heart”). (b) Physical vector graphics (“heart”) with 60 Hz strobe light. (c) Whale (hung by string) and surrounding particles. (d) Whale (hung by string) with projected spout.

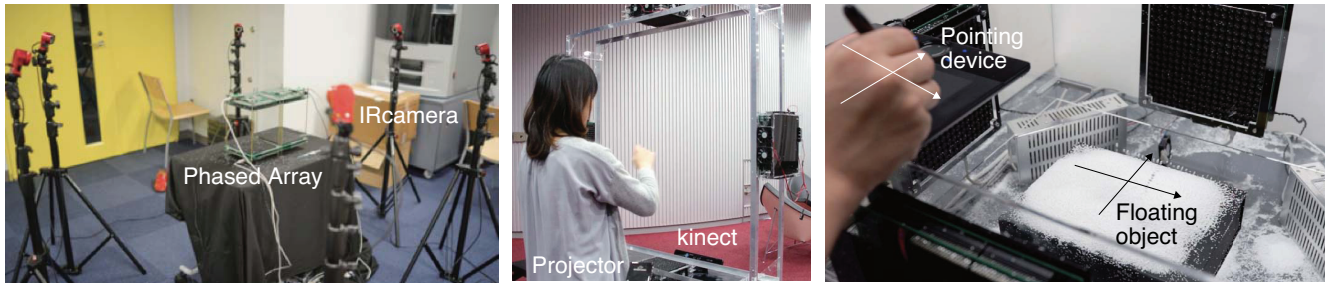


Figure 22: Animation and Interaction. (Left) With IR based motion capture system. (Middle and right) interaction with floated materials.

6.2 Scalability

In this sub-section, we discuss the scalability of our method in terms of the weight and size of objects, the speed of movement, and the number of control channels.

6.2.1 Weight

The intensity of the ultrasound radiated from a single phased array is in proportion to the number of transducers. More transducers enable us to levitate heavier objects. Increasing the number of transducers results in other benefits in addition to higher intensity. One such benefit is a larger workspace keeping the size of the focal point. Another is smaller dispersion of the phase delay characteristics, which leads to more accurate generation and control of the acoustic field.

6.2.2 Size

In Section 6.1, we stated that the size of the object is limited by the frequency. In order to retain its non-audible property, an ultrasonic wave down to 20 kHz (the maximum frequency that humans can sense) is available. We then have a scalability limit of up to 8 mm.

6.2.3 Speed

The maximum manipulation speed of physical vector graphics is 72 cm/s, as mentioned above. Because the workspace is fixed, the acceleration needed to accelerate the object to a given speed is available with a higher intensity of ultrasound.

6.2.4 Multiple controls

In a single wide/narrow acoustic beam of a standing wave, all the levitated objects are manipulated together. Multiple beams are generated, for example, by separating a single phased array into several

regions and controlling them individually. In this way, we can also control multiple clusters of objects individually.

6.3 Setup variations

Our system has a wide range of setup variations at this stage, from $20 \times 20 \text{ cm}^2$ to 100 cm^2 . Larger setups will be possible in the future with larger ultrasonic devices. Figure 23 shows the setup variations.

6.4 Computational potential field

In Section 2.3, we introduced the concept of Computational Potential Field (CPF), which is the source of a noncontact force. This concept not only explains various noncontact forces (such as acoustic, magnetic, and pneumatic) in a unified manner but also serve as a platform for discussing and designing noncontact manipulation in the future. This frees us from specific physical parameters, such as sound pressure, magnetism, and airflow, and allows for discussions based on the divergence, the rotation, the response speed, and the wave/diffusion characteristics of the CPF.

7 Conclusion and future work

In this paper, we reported on a study conducted to expand “graphics” from the digital world to the real world. In the study, 3D acoustic manipulation technology is used to turn real objects into graphical components. The method has wide-ranging applications, such as mid-air projection screen, raster graphics, vector graphics, and real-object animation, with millimeter-sized objects. We implemented these applications using the current version of ultrasonic phased arrays, conducted experimental evaluations, and demonstrated the capabilities of the system. To aid in the explanation of our approach, we also introduced the concept of “computational potential field,” which has the ability to unify all the noncontact manipulation technologies.

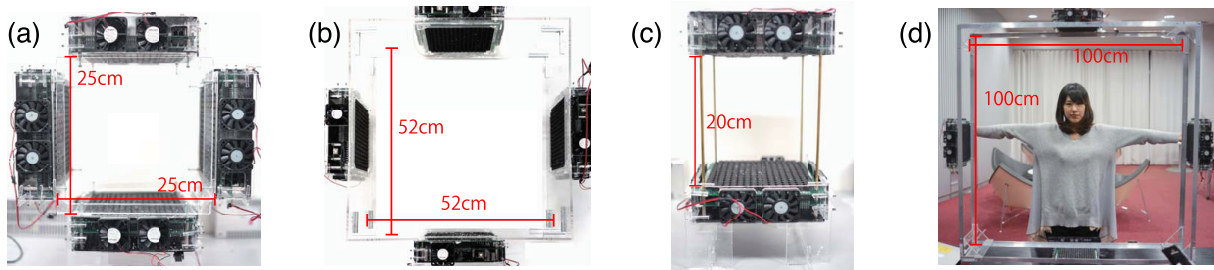


Figure 23: Setup variation. (a) $25 \times 25 \text{ cm}^2$. (b) $52 \times 52 \text{ cm}^2$. (c) $20 \times 20 \text{ cm}^2$. (d) $100 \times 100 \text{ cm}^2$.

Acknowledgements

We would like to express our sincere appreciation to Keita Higuchi, Kensaku Kawauchi, Yui Kita, and Katsuya Fujii, Rekimoto Lab, whose supports and tolerance were considerably valuable in the course of our study. Adding to that we would like to express our sincere appreciation to Ayumi Kato who plays the roll of a photographic model.

References

- BARNUM, P. C., NARASIMHAN, S. G., AND KANADE, T. 2010. A multi-layered display with water drops. *ACM Trans. Graph.* 29, 4 (July), 76:1–76:7.
- BRANDT, E. H. 1989. Levitation in physics. *Science* 243, 4889, 349–55.
- CARTER, T., SEAH, S. A., LONG, B., DRINKWATER, B., AND SUBRAMANIAN, S. 2013. Ultrahaptics: Multi-point mid-air haptic feedback for touch surfaces. In *Proceedings of the 26th Annual ACM Symposium on User Interface Software and Technology*, ACM, New York, NY, USA, UIST ’13, 505–514.
- COSSAIRT, O., NAPOLI, J., HILL, S., DORVAL, R., AND FAVALORA, G. 2007. Occlusion-capable multiview volumetric three-dimensional display. *Applied Optics* 46, 8, 1244–1250.
- FOLLMER, S., LEITHINGER, D., OLWAL, A., HOGGE, A., AND ISHII, H. 2013. inform: Dynamic physical affordances and constraints through shape and object actuation. In *Proceedings of the 26th Annual ACM Symposium on User Interface Software and Technology*, ACM, New York, NY, USA, UIST ’13, 417–426.
- FORESTI, D., NABAVI, M., KLINGAUF, M., FERRARI, A., AND POULIKAKOS, D. 2013. Acoustophoretic contactless transport and handling of matter in air. *Proceedings of the National Academy of Sciences*.
- GOLDSTEIN, S. C., CAMPBELL, J. D., AND MOWRY, T. C. 2005. Programmable matter. *IEEE Computer* 38, 6 (June), 99–101.
- GOR’KOV, L. P. 1962. On the forces acting on a small particle in an acoustical field in an ideal fluid. *Soviet Physics Doklady* 6, 773–775.
- HEINER, J. M., HUDSON, S. E., AND TANAKA, K. 1999. The information percolator: Ambient information display in a decorative object. In *Proceedings of the 12th Annual ACM Symposium on User Interface Software and Technology*, ACM, New York, NY, USA, UIST ’99, 141–148.
- HOSHI, T., TAKAHASHI, M., IWAMOTO, T., AND SHINODA, H. 2010. Noncontact tactile display based on radiation pressure of airborne ultrasound. *IEEE Transactions on Haptics* 3, 3, 155–165.
- HOSHI, T. 2012. Compact ultrasound device for noncontact interaction. In *Advances in Computer Entertainment*, Springer, A. Nijholt, T. Romao, and D. Reidsma, Eds., vol. 7624 of *Lecture Notes in Computer Science*, 502–505.
- ISHII, H., AND ULLMER, B. 1997. Tangible bits: Towards seamless interfaces between people, bits and atoms. In *Proceedings of the ACM SIGCHI Conference on Human Factors in Computing Systems*, ACM, New York, NY, USA, CHI ’97, 234–241.
- ISHII, H., LAKATOS, D., BONANNI, L., AND LABRUNE, J.-B. 2012. Radical atoms: Beyond tangible bits, toward transformable materials. *interactions* 19, 1 (Jan.), 38–51.
- IWAKI, S., MORIMASA, H., NORITSUGU, T., AND KOBAYASHI, M. 2011. Contactless manipulation of an object on a plane surface using multiple air jets. In *ICRA*, IEEE, 3257–3262.
- IWATA, H., YANO, H., NAKAIZUMI, F., AND KAWAMURA, R. 2001. Project feelex: Adding haptic surface to graphics. In *Proceedings of the 28th Annual Conference on Computer Graphics and Interactive Techniques*, ACM, New York, NY, USA, SIGGRAPH ’01, 469–476.
- JONES, A., McDOWALL, I., YAMADA, H., BOLAS, M., AND DEBEVEC, P. 2007. Rendering for an interactive 360° light field display. *ACM Trans. Graph.* 26, 3 (July).
- KIMURA, H., ASANO, A., FUJISHIRO, I., NAKATANI, A., AND WATANABE, H. 2011. True 3d display. In *ACM SIGGRAPH 2011 Emerging Technologies*, ACM, New York, NY, USA, SIGGRAPH ’11, 20:1–20:1.
- KONO, M., KAKEHI, Y., AND HOSHI, T., 2013. lapillus bug. SIGGRAPH Asia 2013 Art Gallery.
- KOZUKA, T., YASUI, K., TUZIUTI, T., TOWATA, A., AND IIDA, Y. 2007. Noncontact acoustic manipulation in air. *Japanese Journal of Applied Physics* 46, 7S, 4948.
- LANDIS, H., 2013. Spaxels. Ars Electronica 2013.
- LEE, C., DiVERDI, S., AND HOLLERER, T. 2009. Depth-fused 3d imagery on an immaterial display. *IEEE Trans. Vis. Comput. Graph.* 15, 1, 20–33.
- LEE, J., POST, R., AND ISHII, H. 2011. Zeron: Mid-air tangible interaction enabled by computer controlled magnetic levitation. In *Proceedings of the 24th Annual ACM Symposium on User Interface Software and Technology*, ACM, New York, NY, USA, UIST ’11, 327–336.
- MARSHALL, M., CARTER, T., ALEXANDER, J., AND SUBRAMANIAN, S. 2012. Ultra-tangibles: Creating movable tangible

objects on interactive tables. In *Proceedings of the SIGCHI Conference on Human Factors in Computing Systems*, ACM, New York, NY, USA, CHI '12, 2185–2188.

NAKAMURA, M., INABA, G., TAMAOKI, J., SHIRATORI, K., AND HOSHINO, J. 2006. Mounting and application of bubble display system: Bubble cosmos. In *Proceedings of the 2006 ACM SIGCHI International Conference on Advances in Computer Entertainment Technology*, ACM, New York, NY, USA, ACE '06.

NIJHOLT, A., GIUSTI, L., MINUTO, A., AND MARTI, P. 2012. Smart material interfaces: "a material step to the future". In *Proceedings of the 1st Workshop on Smart Material Interfaces: A Material Step to the Future*, ACM, New York, NY, USA, SMI '12, 1:1–1:3.

NYBORG, W. L. 1967. Radiation pressure on a small rigid sphere. *Journal of Acoustical Society of America* 42, 947–952.

OCHIAI, Y., HOSHI, T., OYAMA, A., AND REKIMOTO, J. 2013. Poppable display: A display that enables popping, breaking, and tearing interactions with people. In *Consumer Electronics (GCCE), 2013 IEEE 2nd Global Conference on*, 124–128.

OCHIAI, Y., HOSHI, T., AND REKIMOTO, J. 2014. Three-dimensional mid-air acoustic manipulation by ultrasonic phased arrays. *PLoS ONE* 9, 5, e97590.

PERLIN, K., AND HAN, J., 2006. Volumetric display with dust as the participating medium, Feb. 14. US Patent 6,997,558.

POUPYREV, I., NASHIDA, T., MARUYAMA, S., REKIMOTO, J., AND YAMAJI, Y. 2004. Lumen: Interactive visual and shape display for calm computing. In *ACM SIGGRAPH 2004 Emerging Technologies*, ACM, New York, NY, USA, SIGGRAPH '04, 17–.

POUPYREV, I., NASHIDA, T., AND OKABE, M. 2007. Actuation and tangible user interfaces: the vaucausson duck, robots, and shape displays. In *Tangible and Embedded Interaction*, ACM, B. Ullmer and A. Schmidt, Eds., 205–212.

RAKKOLAINEN, I., DIVERDI, S., OLWAL, A., CANDUSSI, N., HÜLLERER, T., LAITINEN, M., PIIRTO, M., AND PALOVUORI, K. 2005. The interactive fogscreens. In *ACM SIGGRAPH 2005 Emerging Technologies*, ACM, New York, NY, USA, SIGGRAPH '05.

SODHI, R., POUPYREV, I., GLISSON, M., AND ISRAR, A. 2013. Aireal: Interactive tactile experiences in free air. *ACM Trans. Graph.* 32, 4 (July), 134:1–134:10.

TOCHKA. Tochka. <http://tochka.jp/> Last accessed on 30 April 2013.

WEBER, R., BENMORE, C., TUMBER, S., TAILOR, A., REY, C., TAYLOR, L., AND BYRN, S. 2012. Acoustic levitation: recent developments and emerging opportunities in biomaterials research. *European Biophysics Journal* 41, 4, 397–403.

WETZSTEIN, G., LANMAN, D., HEIDRICH, W., AND RASKAR, R. 2011. Layered 3d: Tomographic image synthesis for attenuation-based light field and high dynamic range displays. *ACM Trans. Graph.* 30, 4 (July), 95:1–95:12.

WHYMARK, R. 1975. Acoustic field positioning for containerless processing. *Ultrasoundics* 13, 6, 251 – 261.

XIE, W. J., CAO, C. D., LU, Y., HONG, Z. Y., AND WEI, B. 2006. Acoustic method for levitation of small living animals. *Applied Physics Letters* 89, 21 (Nov), 214102–214102–3.

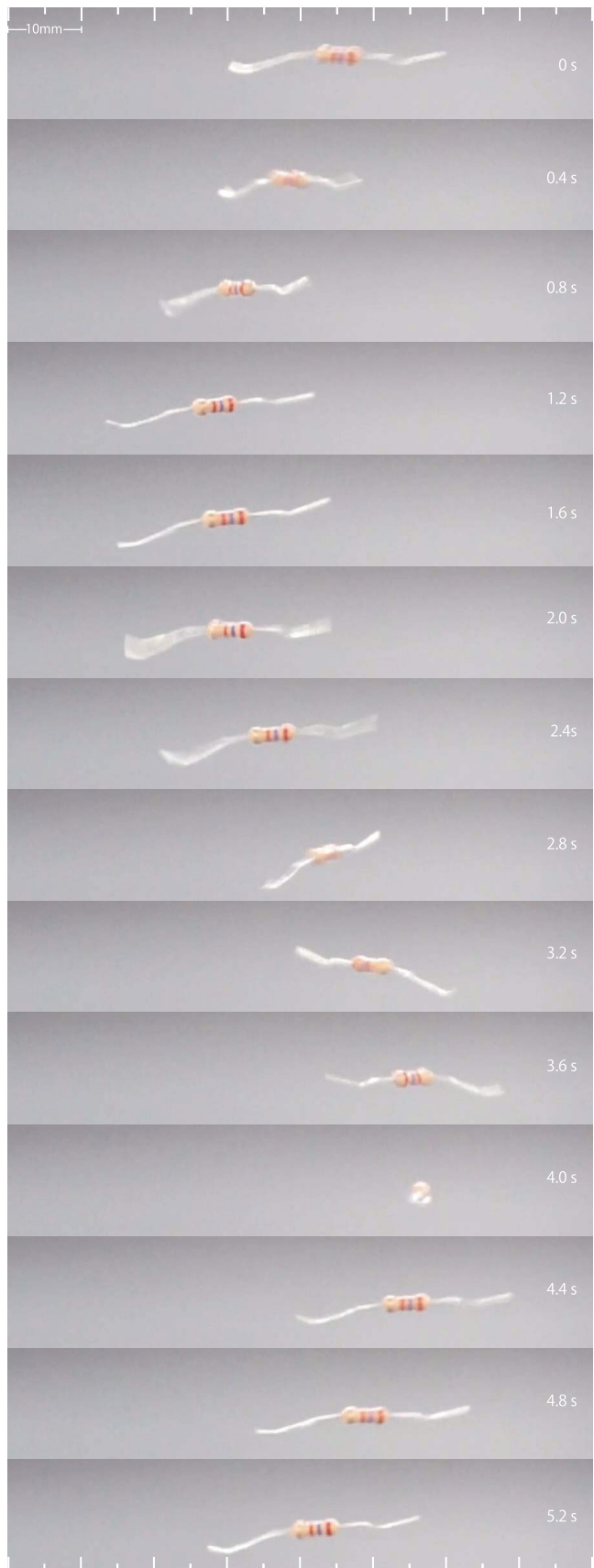


Figure 24: Time-series photographs of animation of a floated object (0.25-W carbon resistor).